



Determining maximum entropy in 3D remote sensing height distributions and using it to improve aboveground biomass modelling via stratification

Syed Adnan^{a,*}, Matti Maltamo^a, Lauri Mehtätalo^b, Rhei N.L. Ammaturo^c, Petteri Packalen^a, Rubén Valbuena^{d,*}

^a University of Eastern Finland, School of Forest Sciences, PO Box 111, FI-80101 Joensuu, Finland

^b University of Eastern Finland, School of Computing, P.O. Box 111, FI-80101 Joensuu, Finland

^c University of Cambridge, Department of Plant Sciences, Forest Ecology and Conservation, Downing Street, CB2 3EA Cambridge, UK

^d Bangor University, School of Natural Sciences, Thoday building, Bangor, Gwynedd LL57 2UW, UK

ARTICLE INFO

Editor: Jing M. Chen

Keywords:

Forest structure
Forest aboveground biomass
Gini coefficient
L-moments
Airborne laser scanning

ABSTRACT

McArthur's foliage height diversity (FHD) has been the gold standard in the determination of structural complexity of forests characterized by LiDAR vertical height profiles. It is based on Shannon's entropy index, which was originally designed to describe evenness in abundances among qualitative typologies, and thus the calculation of FHD involves subjective layering steps which are essentially unnatural to describe a continuous variable (X) such as height. In this contribution we aim to provide a mathematical framework for determining maximum entropy in 3D remote sensing datasets based on the Gini Coefficient of theoretical continuous distributions, intended to replace FHD as entropy measure in vertical profiles of LiDAR heights (1D, X), with extensions to variables expressing dimensions of higher order (2D or 3D, $Z \propto X^2$ or X^3). Then we apply this framework to Boreal forests in Finland to describe landscape heterogeneity with the intention to improve the modelling of forest aboveground biomass (AGB), hypothesizing that LiDAR models of AGB should essentially be different in areas of differing structural characteristics. We carried out a pre-stratification of LiDAR data collected in 2012 using simple rules applied to the L-skewness (L_{skew}) and L-coefficient of variation of LiDAR echo heights (L_{cv} ; equivalent to the Gini coefficient, GC_H), determining a new threshold at $GC_H = 0.33$ as a consequence of the newly developed mathematical proofs. We observed only moderate improvements in terms of model accuracies: RMSDs reduced from 41.7% to 38.9 or 37.0%. More remarkably, we identified critical differences in the metrics selected at each stratum, which is useful to understand what predictor variables are more important for estimating AGB at each area of a forest. We observed that higher LiDAR height percentiles are more relevant at open canopies and heterogeneous forests, whereas closed canopies in homogeneous forests obtain most accurate predictions from a combination of cover metrics and percentiles around the median. Without stratification, the overall model would neglect explained variability in the structural types of lower occurrence, and predictions from a model influenced by structural types of higher occurrence would be biased at those areas. These results are thus useful in terms of improving our understanding on the relationships underlying LiDAR-AGB models.

1. Introduction

Structural complexity is an essential morphological trait of ecosystems, complementary to others like vegetation height or cover (Schneider et al., 2017; Fahey et al., 2019; Valbuena et al., 2020), which is relevant to various ecological processes such as nutrients cycling, carbon sequestration and species interactions (Brokaw and Lent, 1999; Lindenmayer et al., 2000; McElhinny et al., 2005). There is however a

lack of consensus on the most appropriate means to measure the structural complexity of ecosystems (Neumann and Starlinger, 2001; Lexerød and Eid, 2006), with approaches focused on measuring either entropy, e.g. Simpson or Shannon indices (McArthur and McArthur, 1961), or variability, e.g. variance or Gini coefficient (GC) (Gini, 1921; Weiner, 1990). The most popular approach follows the early works of McArthur and McArthur (1961) who calculated the Shannon-based foliage height diversity (FHD) after layering the ecosystem vertical profile into three

* Corresponding authors.

E-mail addresses: adnan@uef.fi (S. Adnan), matti.maltamo@uef.fi (M. Maltamo), lauri.mehtatalo@uef.fi (L. Mehtätalo), nla32@cam.ac.uk (R.N.L. Ammaturo), petteri.packalen@uef.fi (P. Packalen), r.valbuena@bangor.ac.uk (R. Valbuena).

<https://doi.org/10.1016/j.rse.2021.112464>

Received 26 June 2020; Received in revised form 9 April 2021; Accepted 17 April 2021

Available online 23 April 2021

0034-4257/© 2021 Elsevier Inc. All rights reserved.

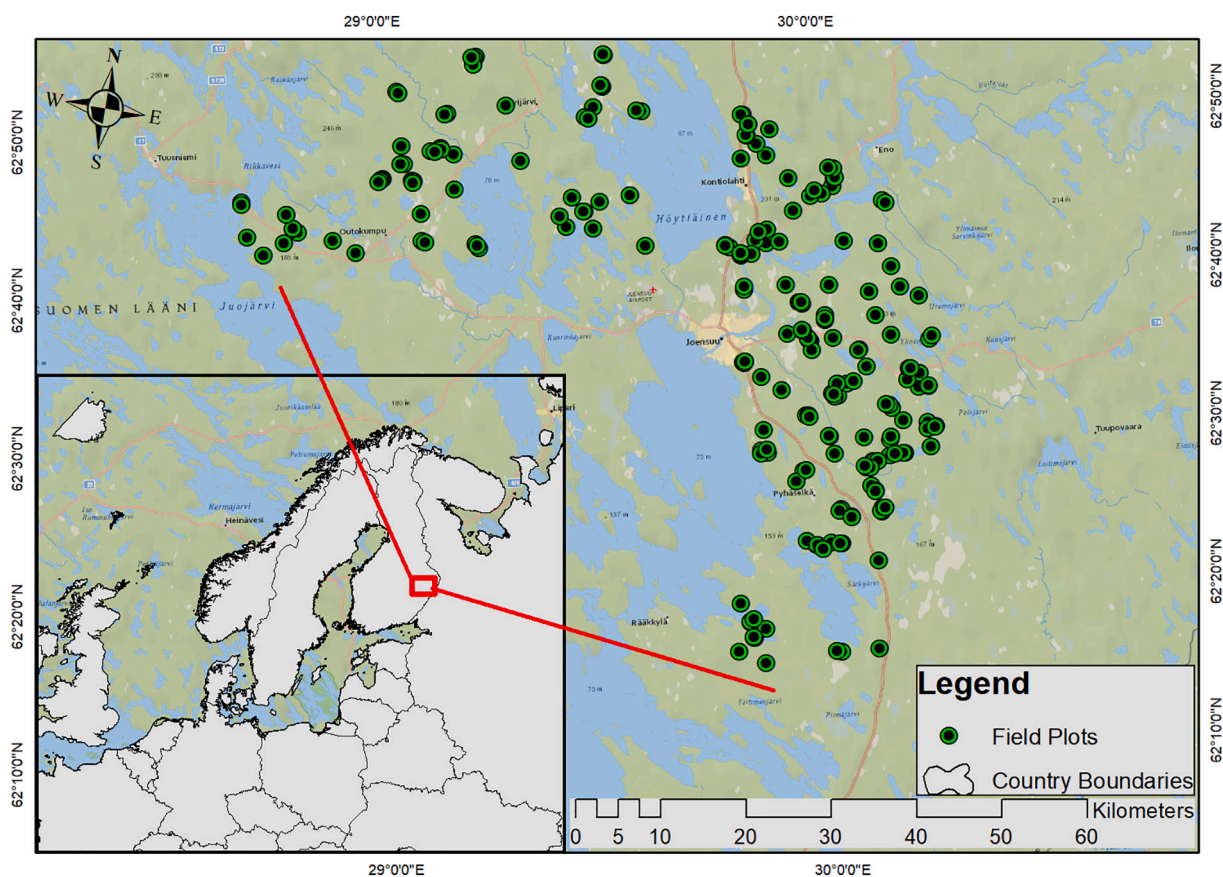


Fig. 1. Map of the North Karelia Region, Finland (study area).

strata, but there have been pleas for alternative measures (Lovejoy, 1972; Pearson, 1975; Erdelen, 1984; Weiner and Thomas, 1986; Valbuena et al., 2012). This dichotomy has been reflected in the derivation of structural complexity measures from LiDAR, with alternatives based on either layering the vertical profile (Lefsky et al., 2002a; Vierling et al., 2008; Simonson et al., 2014; Weisberg et al., 2014; Listopad et al., 2015; Wilkes et al., 2016; Almeida et al., 2019a; Bakx et al., 2019) or measuring variability in LiDAR heights (Valbuena et al., 2017a; Moran et al., 2018; Mononen et al., 2018; Crespo-Peremarch et al., 2020; Hagar et al., 2020).

In this contribution we propose a mathematical framework (Appendix A) which effectively merges both approaches, by showing how maximum entropy can be flagged up from values of a variability measure such as the Gini coefficient. They constitute formal deductive proofs of ideas that have previously been presented on the basis of empirical indications such as a threshold at $GC = 0.5$ employed to discriminate ecosystem structural heterogeneity (Valbuena et al., 2012, 2017a). Based on these mathematical developments, we further argue that different thresholds apply for GC depending on whether calculated from LiDAR heights (GC_H), or tree basal areas (GC_{BA}), because the former is a variable representing one dimension (X) and the latter is an area, and thus bi-dimensional (X^2) (Appendix A). This mathematical framework thus provides unified means for determining maximum entropy in the 3D space of information provided by remote sensing tools such as LiDAR.

To quantify the amount of carbon sequestered by forests over large geographical areas, and use them to inform global policies, it is important to attain reliable estimations of forest aboveground biomass (AGB) from local to global scales (Gibbs et al., 2007). In this context, remote sensing in general, and LiDAR in particular, are the key technologies to monitor reductions in emissions of greenhouse gases from deforestation and forest degradation (REDD) (Boudreau et al., 2008; Asner et al.,

2010). Airborne LiDAR produces detailed canopy information (Maltamo et al., 2005; Gobakken and Næsset, 2008) that provides opportunities for predicting accurately various ecosystem attributes such as vegetation height (Magnussen et al., 1999; Maltamo et al., 2004; Koukoulas and Blackburn, 2005), tree diameters (Næsset, 2002; Rätty et al., 2018), structural heterogeneity (Vierling et al., 2008; Weisberg et al., 2014; Adnan et al., 2019), tree species (Van Aardt et al., 2008), or forest biomass and carbon (Næsset and Gobakken, 2008; Kronseder et al., 2012; Valbuena et al., 2017b). Metrics derived from airborne LiDAR are the most promising information for efficient and accurate AGB prediction (Asner and Mascaro, 2014; Bouvier et al., 2015; Longo et al., 2017). For this reason, these metrics are employed as auxiliary variables in airborne LiDAR-assisted estimations (Gobakken and Næsset, 2008; Asner et al., 2010). Mehtätalo and Nyblom (2009, 2012) developed the relationship between canopy height obtained from airborne LiDAR data and forest attributes such as stand density and mean tree height, improving model-based estimations. However, we still lack information on the relationship between LiDAR metrics with the forest AGB, and how the predictive models are affected by forest structures (Drake et al., 2003; Knapp et al., 2020).

Researchers have developed a wide variety of LiDAR models estimating AGB stocked in forests (Zolkos et al., 2013). The prediction error of the total AGB is dependent on the relationship between foliage observed by LiDAR and various AGB components (Lefsky et al., 2002b; Næsset and Gobakken, 2008; Hernando et al., 2019). Thus, high heterogeneity in the structural complexity of forests may cause difficulties in modelling (Drake et al., 2003; Hall et al., 2005; Jaskierniak et al., 2011; Vincent et al., 2014). While there have been many attempts to generalize LiDAR modelling of AGB (Asner and Mascaro, 2014; Bouvier et al., 2015), a general relationship may not be appropriate for all regions, both even and uneven sized forests or dense and sparse spatial structures (Vincent et al., 2014; Häbel et al., 2019; Knapp et al., 2020).

To overcome this difficulty, the forest area can be stratified into different development classes (Næsset, 2002) or forest structural types (FSTs) (Mascaro et al., 2011; Vincent et al., 2014), and a separate model can be applied to each of them to obtain more reliable AGB estimations. With these regards, we hypothesized that the Gini coefficient can be useful for such FST stratification prior to modelling the forest AGB. Bollandsås and Næsset (2007) obtained reliable results following such approach with the support of field information (i.e., GC_{BA}). Alternatively, we postulated that these FSTs could be detected directly from airborne LiDAR data (i.e. GC_H), and apply a separate AGB model in each FST to improve AGB predictions. Based on results in Valbuena et al. (2017a), we considered the use of L-moment ratios for such stratifications: L-coefficient of variation of LiDAR echo heights (L_{cv} ; equivalent to the Gini coefficient, GC_H) and L-skewness (L_{skew}). We considered a new threshold at $GC_H = 0.33$ for separating even sized from uneven sized forest structures, based on findings in Appendix A. Furthermore, Valbuena et al. (2017a) also identified FSTs according to their light environment characteristics using the $L_{skew} = 0$ threshold which segregate the euphotic/open canopy and oligophotic/closed canopy forest areas (Lefsky et al., 2002a), by separating them as positive and negative skewness in between the $[-1,1]$ bounds of L_{skew} . We evaluated the potential of these detected FSTs in improving the AGB prediction from the airborne LiDAR data.

In this article, we set the mathematical foundations for determining maximum entropy from a distribution of heights in 3D remote sensing (Appendix A), as an alternative to common binning procedures employed to determine McArthur and McArthur's (1961) FHD. Then we employed this rationale, stratified the LiDAR-surveyed area according to the $L_{cv} = 0.33$ and $L_{skew} = 0$ rules following Valbuena et al. (2017a), and carried out stratified sampling with roughly equal sample sizes within each FST. The aim of this stratification was to evaluate the potential of FSTs to improve forest AGB predictions in the pre-stratified airborne LiDAR data compared to the AGB predictions in the whole dataset without pre-stratification. We developed a general LiDAR-AGB model for the whole dataset without pre-stratification, and separate FST-specific models at each stratum. We hypothesized that LiDAR models predicting AGB should essentially be different in areas of differing structural characteristics. For this reason, we also paid careful attention to the LiDAR metrics selected at each model, and used those results to make inferences on the relationship behind the choice of metrics at each forest area, with the intention to shed light on the effects of forest heterogeneity on LiDAR models predicting AGB.

2. Material and methods

2.1. Study area and data collection

This study was conducted in a 252,000 ha boreal forest located in the North Karelia region of Finland (Fig. 1). The dominant species in the study area are Norway spruce (*Picea abies* (L.) Karst.), Scots pine (*Pinus sylvestris* L.) and Birch species (*Betula* spp.), and some other deciduous species such as *Alnus* spp. and *Populus* spp. are also present. In May 2012, a Leica ALS60 laser scanning system was used to collect airborne LiDAR data. Flight elevation was 2300 m above ground level, which resulted in a scan density of 0.91 pulses per square meter. The digital terrain model with 2 m resolution derived from the same LiDAR dataset was provided by National Land Survey (Finland). The DTM was subtracted from the LiDAR echo heights and area-based LiDAR metrics were computed using the FUSION software (Version 3.70, USDA Forest Service; McGaughey, 2019). With the intention to get in the full structural characteristics of forests and commensurate with forest data acquisition, a very small height threshold (< 0.1 m) was used to exclude ground echoes in the computation of area-based metrics (Görgens et al., 2017). This eliminates ground echoes but consider seedlings and saplings, which were included in the field inventory (Valbuena et al., 2016). Among the set of FUSION metrics, two L-moment ratios were used for simulating a pre-

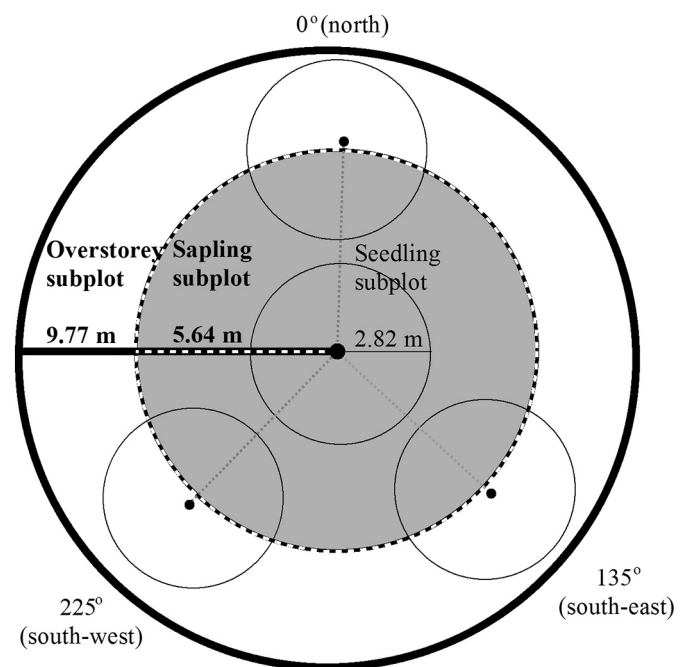


Fig. 2. Plot design for field data collection.

stratification: L-coefficient of variation (L_{cv}) and L-skewness (L_{skew}). The remaining metrics were involved in the modelling of AGB.

Field data for the calibration/validation of AGB models were jointly collected by the Finnish Forest Centre (Suomen Metsäkeskus; SMK) and University of Eastern Finland (UEF) in 2013 (Valbuena et al., 2017a). There were 244 field plots in total from eight different strata and sample size was approximately equal in each stratum. The stratification was based on the forest development classes – seedling, sapling, young, advanced, mature, shelterwood, seed-tree and multi-storey (Valbuena et al., 2016) –, determined on the basis of the SMK stand-wise information from the previous forest management plan, randomly selecting plot locations over areas covering each development class. Field data acquisition consisted in a concentric circle design, recording species and diameter at breast height (dbh ; cm) of trees within each concentric plot according to its size (Valbuena et al., 2016). Tree heights (h ; m) were measured only for the basal area median tree of each species. For the even sized development classes (young, advanced and mature), the field data were collected by SMK using a plot size of 9 m radius for trees with $dbh > 8$ cm, while saplings were recorded within 5.64 m radius and seedlings were counted using a 2.82 m long stick in distributed sub-plots (Fig. 2). Plots within the seed tree, shelterwood and multi-storey development classes were collected by UEF using the same plot design. However, the size of the outer plot in these three development classes was slightly increased to 9.77 m so that its size would become integer multiplier of the inner subplots, which is convenient for the calculation of GC_{BA} following Valbuena et al. (2013). For visual comparison of these development classes, mean leaf area density (LAD) vertical profiles with 95% confidence intervals from all plots within each development class were calculated from LiDAR data using the R package LeafR (Almeida et al., 2019b).

2.2. Rule-based stratification of forest structural types using airborne lidar data

Postulating that LiDAR models of AGB should be essentially different in areas of differing structural characteristics, we employed this dataset to simulate a pre-stratification scenario by classifying the prediction area into FSTs detected directly from the LiDAR data. The study area was stratified using the abovementioned two L-moment ratios of airborne

Table 1
Aboveground biomass and other forest attributes calculated at each forest development class.

Development Class			AGB (Mg·ha ⁻¹)	QMD (cm)	GC _{BA}	N (trees·ha ⁻¹)	GC _H /L _{cv}	L _{skew}
Seedlings	Min		2.48	0.10	0.00	13,909	0.07	0.14
	Mean		7.96	0.10	0.00	44,770	0.23	0.31
	Max		28.51	0.10	0.00	182,522	0.54	0.70
Saplings	SD		5.14	0.00	0.00	32,987	0.09	0.13
	Min		6.14	0.10	0.00	1601	0.20	-0.18
	Mean		34.88	3.05	0.35	31,852	0.42	0.21
Young	Max		112.48	6.93	0.89	110,774	0.60	0.59
	SD		24.62	1.78	0.29	24,754	0.12	0.20
	Min		13.09	6.23	0.25	864	0.15	-0.36
Advanced	Mean		79.91	10.00	0.43	3254	0.29	-0.11
	Max		160.01	14.44	0.66	6523	0.58	0.33
	SD		31.67	2.18	0.09	1475	0.11	0.17
Mature	Min		49.56	12.68	0.15	314	0.09	-0.41
	Mean		96.98	17.27	0.42	1003	0.28	-0.20
	Max		182.76	22.15	0.63	2082	0.50	0.14
Shelterwood	SD		30.26	2.63	0.14	462	0.10	0.13
	Min		73.75	16.07	0.19	314	0.09	-0.48
	Mean		179.07	23.35	0.49	844	0.23	-0.21
Seed Trees	Max		410.55	32.44	0.68	1807	0.41	0.00
	SD		76.81	4.60	0.17	374	0.08	0.11
	Min		23.15	3.32	0.79	9020	0.21	-0.36
Multi-Storied	Mean		171.01	5.63	0.95	33,935	0.36	0.07
	Max		305.34	9.25	1.00	108,805	0.57	0.26
	SD		83.39	1.65	0.06	24,028	0.10	0.15
Multi-Storied	Min		23.65	2.29	0.11	117	0.14	-0.23
	Mean		70.43	14.76	0.73	9833	0.58	0.37
	Max		143.52	38.14	0.99	39,601	0.85	0.90
Multi-Storied	SD		28.29	12.14	0.35	11,209	0.21	0.31
	Min		17.99	1.41	0.68	2219	0.20	-0.22
	Mean		77.02	3.87	0.92	33,279	0.58	0.30
Multi-Storied	Max		271.39	9.60	0.99	78,131	0.84	0.83
	SD		54.73	2.19	0.09	16,382	0.16	0.30

AGB: aboveground biomass; QMD: quadratic mean diameter; GC_{BA}: Gini coefficient of basal area; GC_H: Gini coefficient of LiDAR; L_{cv}: L-coefficient of variation of LiDAR heights; L_{skew}: L-skewness of LiDAR heights SD: standard deviation.

LiDAR height distributions, and the rules were deduced from their mathematical properties instead of inductive statistical distributions or supervised classification, thus absence of any field information is involved (Valbuena et al., 2016). As L_{cv} is mathematically equivalent to the Gini coefficient of LiDAR echo heights (GC_H) (Valbuena et al., 2017a), it could be used to describe the structural properties related to the inequality in tree sizes within a forest area. L_{cv} = 0.33 was used as a boundary line to discriminate forests with even-sized FSTs (L_{cv} < 0.33) from uneven-sized ones (L_{cv} > 0.33), on the grounds that maximum entropy in the distribution of LiDAR heights is reached at L_{cv} = 0.33 (Appendix A). Similarly, asymmetry (L_{skew}) describes the structural heterogeneity related to light availability and tree size dominance (Valbuena et al., 2017a). L_{skew} = 0, which represents the symmetric distribution of LiDAR echo heights, was used to separate forests having oligophotic areas/closed canopy (L_{skew} < 0) from euphotic areas/open canopy areas (L_{skew} > 0) (Lefsky et al., 2002a).

2.3. Aboveground biomass calculation from field data

R statistical software (R Core Team, 2019) was used for all statistical analyses and modelling. Locally developed species-specific biomass equations were used to calculate tree above-ground biomass (agb; kg) for Scots pine and Norway spruce (Repola, 2009), and another for birch (Repola, 2008) which was used for all deciduous species. These were based on dbh and h, and thus individual tree heights were subsequently predicted using the Näslund (1936) height curve:

$$h = 1.3 + \left(\frac{dbh}{\beta_0 + \beta_1 dbh} \right)^\alpha, \quad (1)$$

where the exponent was $\alpha = 2$ for pine and deciduous species, and $\alpha = 3$ for spruce. We followed the methods suggested by Siipilehto (1999) in the estimation the Näslund's height curve model parameters (β_0 , β_1) for

each species which included plot-level calibration with species-specific diameter (\tilde{D}_{ba}) and height (\tilde{H}_{ba}) of the tree with median basal area (\tilde{ba}). Then the species-specific parameters were used in the height curve model to predict the missing tree heights from their dbh. Once calculated all the tree level agb values, they were aggregated to plot level (AGB; Mg·ha⁻¹) according to their corresponding hectare expansion factors, and used as a response variable in subsequent LiDAR models.

2.4. Modelling of aboveground biomass from airborne LiDAR data

Many airborne LiDAR derived metrics (predictors) were available for modelling the AGB. We used function "regsubset" of the R package "leaps" (Lumley and Miller, 2017), which performed a selection of the best subset of predictors using an exhaustive search among typical LiDAR-AGB models (Valbuena et al., 2017b). We made an independent selection, the best subset of predictors for the general model including the whole dataset (i.e. without stratification), and also for each FST-specific model (even versus uneven sized forest structures, and euphotic/open canopy versus oligophotic/closed canopy areas). Thereafter, modelling based on the k-nearest neighbor (k-NN) method was used to predict the response variable (AGB) from the best subset of airborne LiDAR predictors (Mcinerney et al., 2010). We used Euclidean distance with k = 5 in the k-NN implementation available in the R package "Yalmpute" (1.0–31 version; Crookston and Finley, 2008).

2.5. Accuracy assessment of aboveground biomass prediction

We used a 10-fold cross validation method for assessing the accuracy of the resulting models. The results of the general model and FST-specific models were evaluated and compared by means of their mean difference (MD) and root mean square difference (RMSD):

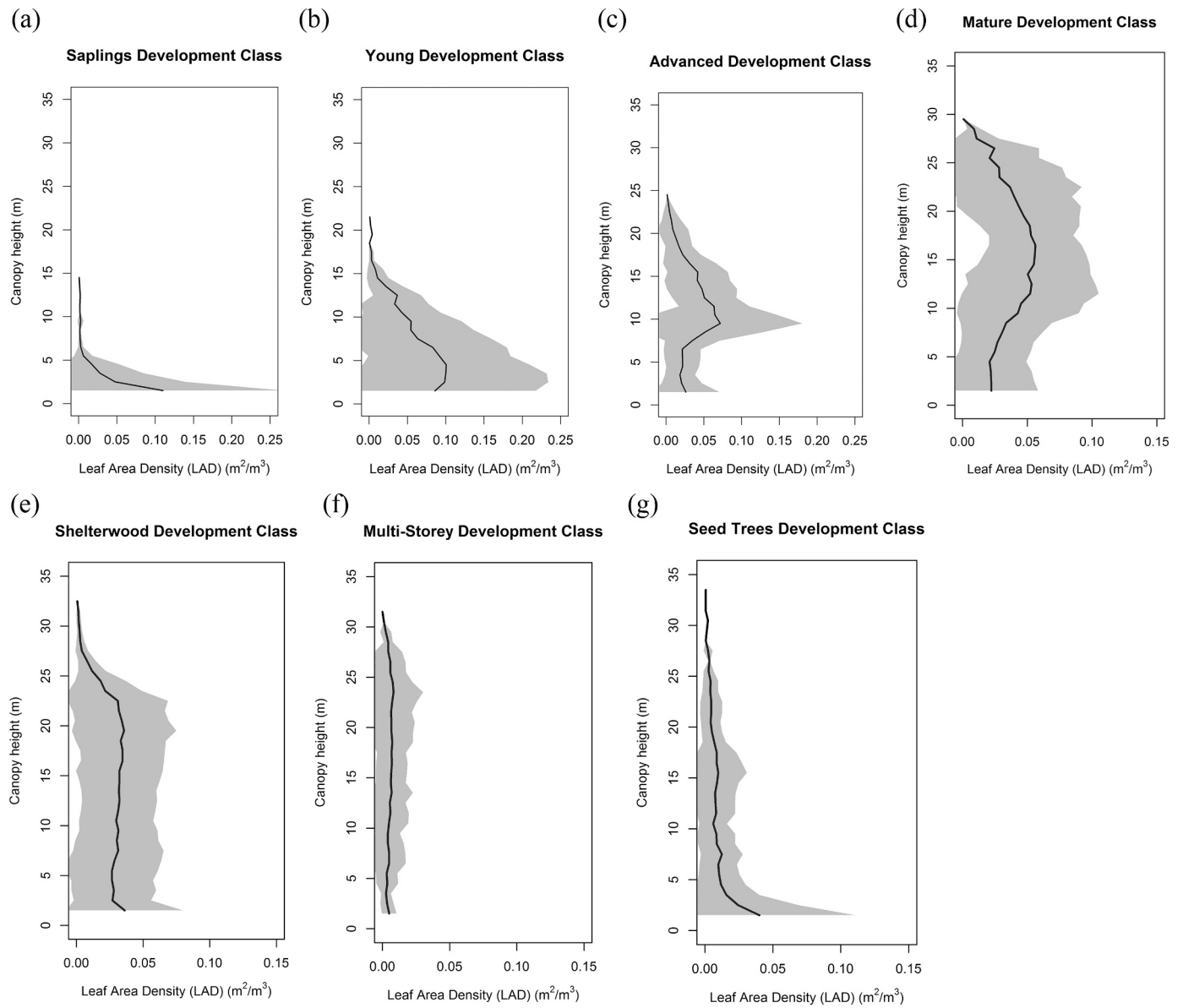


Fig. 3. Mean leaf area density (LAD) profiles calculated directly from LiDAR data for each development class (a) Sapling (b) Young (c) Advanced (d) Mature (e) Shelterwood (f) Multi-storey and (g) Seed trees. Lines show mean LAD of all plots and grey areas their 95% confidence intervals.

$$RMSD = \sqrt{\frac{\sum_{i=1}^n \left(\left(y_i^{cv} - \hat{y}_i \right)^2 \right)}{n}}, \quad (2)$$

$$MD = \frac{\sum_{i=1}^n \left(\left(y_i^{cv} - \hat{y}_i \right) \right)}{n}, \quad (3)$$

where n is the total number of observations (field plots), y_i^{cv} and \hat{y}_i are the predicted and observed value of AGB for observation i , respectively. Relative values (%) of MD and $RMSD$ were obtained as the percentage over the mean observed AGB. As an additional quality control measure, we used a hypothesis test on the 1:1 correspondence between the observed (obs_i) and predicted (pre_i^{cv}) values from the intercept (α) and slope (β) of their linear regression (Leite and Tavares de Oliveira, 2002; Piñeiro et al., 2008),

$$obs_i = \alpha + \beta pre_i^{cv}, \quad (4)$$

To avoid overfitting the models to the sample, the best subset procedure was constrained by additional restrictions to the sum of squares ratio (SSR), which evaluates the inflation in the unexplained variance when the model is not cross-validated (Valbuena et al., 2017b). SSR is the ratio between the squared root sum of the squares obtained by cross validation (SS^{cv}) and without cross validation (SS^{fit}).

$$SSR = \sqrt{SS^{cv}} / \sqrt{SS^{fit}}, \quad (5)$$

$$SS^{cv} = \sum_{i=1}^n \left(y_i^{cv} - \hat{y}_i \right)^2 \quad (6)$$

$$SS^{fit} = \sum_{i=1}^n \left(y_i^{fit} - \hat{y}_i \right)^2 \quad (7)$$

Where, \hat{y}_i is the observed value of the AGB for observation i , and y_i^{cv} and y_i^{fit} are the predicted values using cross validation and without cross validation, respectively.

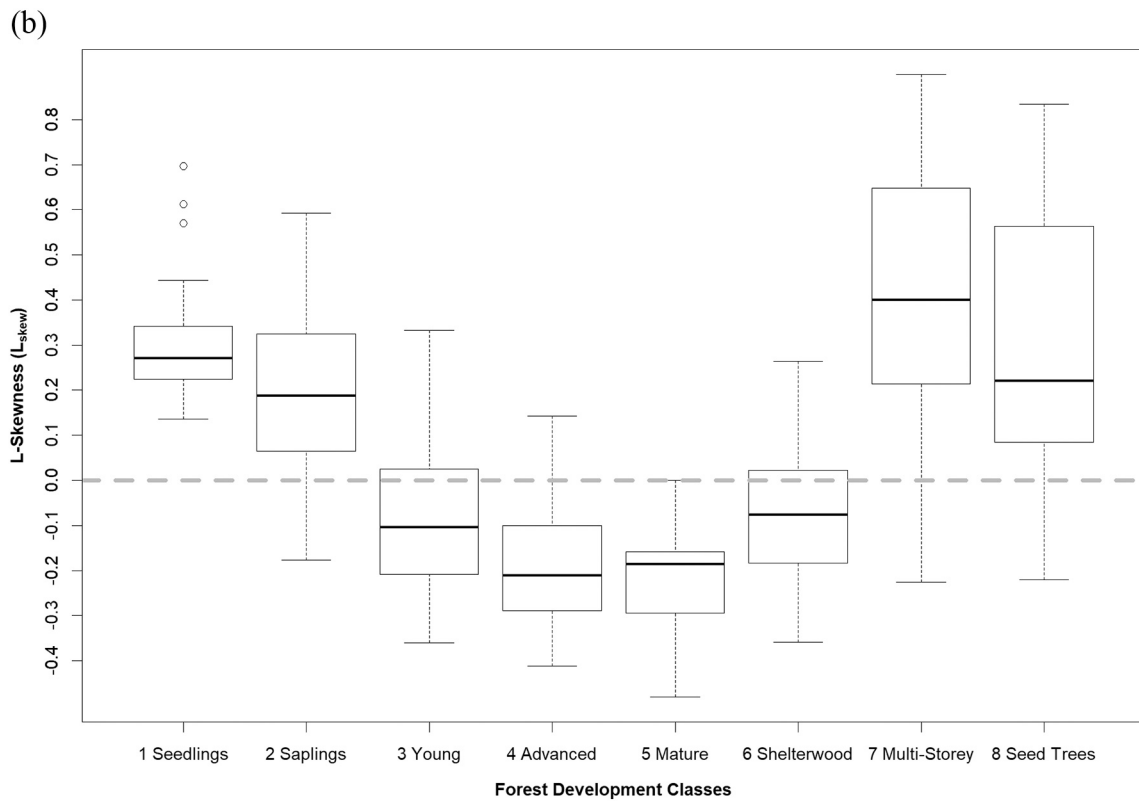
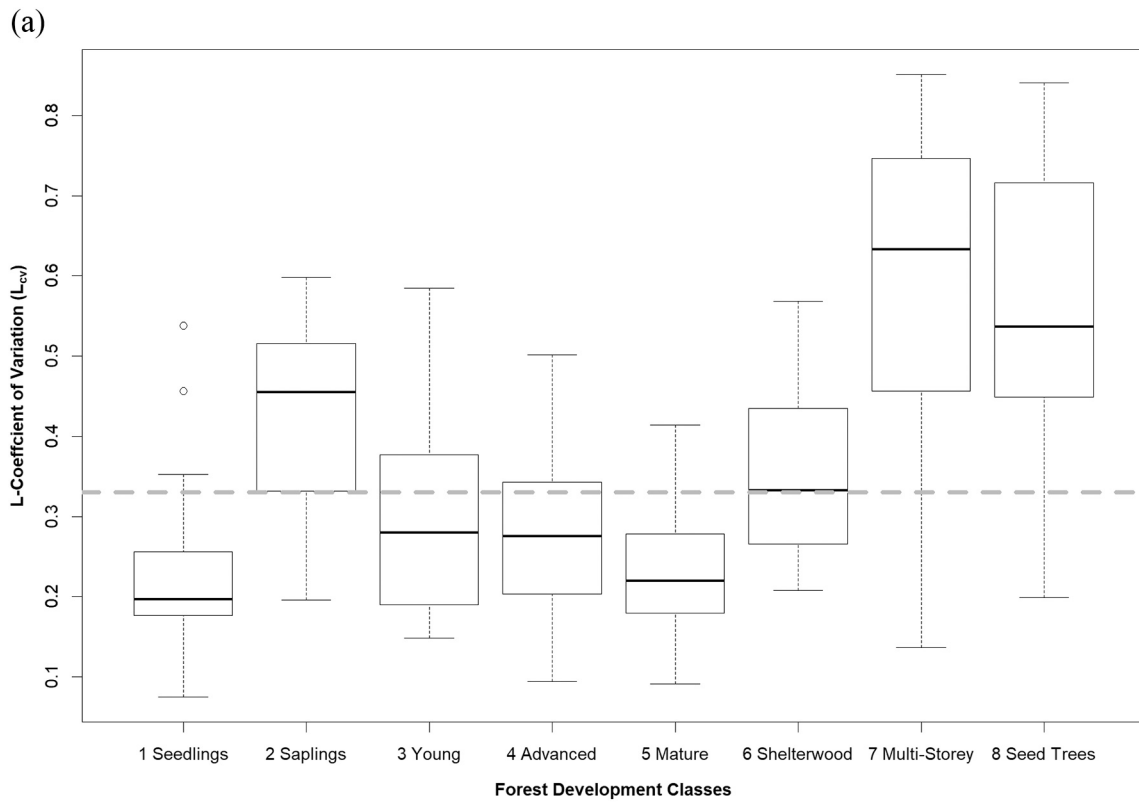


Fig. 4. Distribution of different forest development classes on either side of the (a) $L_{Cv}(GC_H) = 0.33$ and (b) $L_{skew} = 0$.

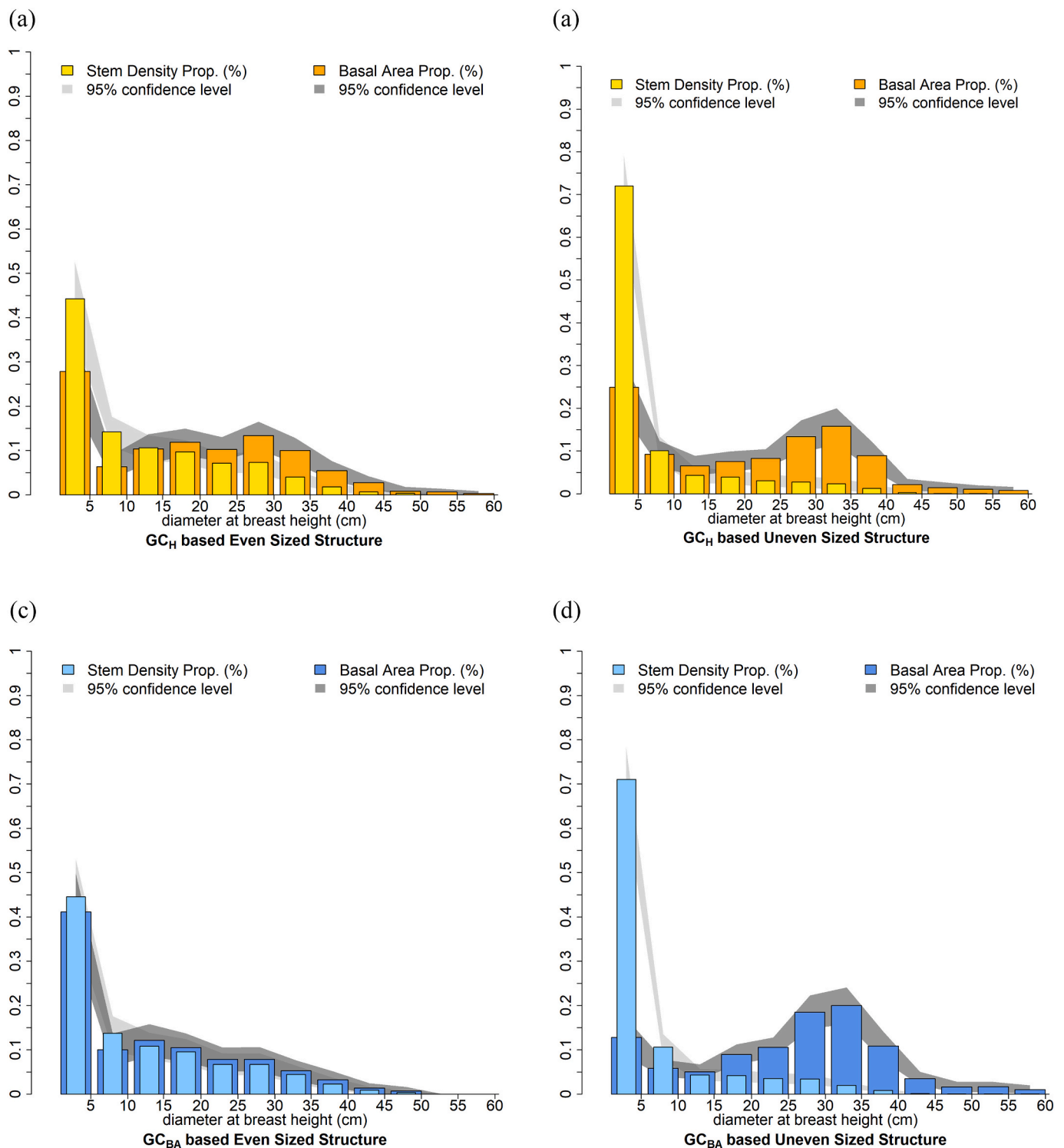


Fig. 5. Comparison of diameter and basal area distribution in the even and uneven sized forest structural types separated by Gini coefficient of LiDAR ($GC_H(L_{cv}) = 0.33$) (a, b) and Gini coefficient of basal area ($GC_{BA} = 0.5$) (c, d).

3. Results

3.1. Airborne LiDAR based forest structural types

Table 1 gives a development class-wise summary of plot-level characteristics calculated from the field data – density (N), quadratic mean diameter (QMD), above ground biomass density (AGB) and Gini coefficient of basal area (GC_{BA}) –, and also from the LiDAR data – L-coefficient

of variation (L_{cv} ; equivalent to the Gini coefficient, GC_H) and L-skewness (L_{skew}). of LiDAR return heights –. Height profiles of each development class calculated from LiDAR data are given in Fig. 3, which shows mean changes in LAD through the vertical profiles at each development class. Fig. 4 further shows how different forest structural types detected directly from airborne LiDAR data are distributed either sides of the $L_{cv}(GC_H) = 0.33$ and $L_{skew} = 0$ thresholds. Some structural dynamics can be observed from these figures, since the majority of areas in seedling

Table 2

Airborne LiDAR predictors selection (best subset) for the general model (whole data without pre-stratification) and each forest structural type specific model (even sized, uneven sized, oligophotic/closed canopy and euphotic/open canopy forest structures).

Predictors	General Model	$GC_H(L_{cv})$		L_{skew}	
		Even (<0.33)	Uneven (>0.33)	Oligophotic (<0)	Euphotic (>0)
Variance	*		*		*
Median of the absolute deviations (MAD) from the overall mode	*	*		*	
MAD from the overall median					*
L.skewness		*			
Average absolute deviation (AAD)			*		
Cubic mean					*
Quadratic mean		*			
25th height percentile	*				
50th height percentile	*	*		*	
60th height percentile					*
70th height percentile			*		
99th height percentile			*		*
% first returns above 0.1 m			*		
% all returns above 0.1 m				*	
% all returns above mean				*	
% first returns above mode		*		*	
Ratio returns above 0.1 m /total first returns	*	*	*		*
Canopy relief ratio	*			*	

development classes were separated as even sized by $L_{cv}(GC_H) < 0.33$, because they are very small and roughly equal in size at first, to later more inequality in diameter distribution toward the sapling stage ($L_{cv}(GC_H) > 0.33$) (Fig. 4a). Likewise, the young, advanced and mature development classes which mostly contain equality in diameter/basal area distribution were mostly separated as even sized ($L_{cv}(GC_H) < 0.33$). Seed trees and multi-storied development classes have higher inequality in their diameter distribution, they show high dispersion in their LiDAR echoes, and thus they were separated as uneven sized structure ($L_{cv}(GC_H) > 0.33$). Similarly, in Fig. 4b most seedling and sapling development classes were separated as euphotic areas ($L_{skew} > 0$) because their canopies have not closed yet at these stages of development. As they grow and increase in AGB through young, advanced and mature development classes, they shift toward oligophotic areas with closed canopies and negative skewness of LiDAR return heights ($L_{skew} < 0$). The shelterwood development class which has a dense overstory and high LiDAR returns was classified as oligophotic ($L_{skew} < 0$), whereas seed-tree areas and multi-storey development classes with sparse overstorey were mainly classified as euphotic ($L_{skew} > 0$).

We were then interested on whether the different thresholds that Appendix A shows for LiDAR heights ($GC_H(L_{cv}) = 0.33$) and field data ($GC_{BA} = 0.5$) would segregate forests with similar structural properties. Fig. 5 shows a comparison of aggregated diameter distributions (plus basal area-weighted distributions, in darker colors in the background) with confidence intervals. The difference between the distribution of proportions in density of stems versus basal area highlights structural differences which cannot be easily appreciated in diameter distributions, since in highly complex structures with large differences in tree sizes the proportion of basal area taken by larger trees becomes predominant. This could be appreciated in the distributions of strata

yielded from the LiDAR data only ($GC_H(L_{cv}) < 0.33$ and $GC_H(L_{cv}) > 0.33$, respectively in Fig. 5a and b), as much as it was for the distributions yielded when the strata was generated using the field data itself ($GC_{BA} < 0.50$ and $GC_{BA} > 0.50$, respectively in Fig. 5c and d). These results emphasize the reliability of a purely LiDAR-based classification in the structural heterogeneity assessment of forests.

3.2. Best-subset variable selection

In order to facilitate direct comparison of all models, we fixed the number of LiDAR predictors to be six for all models, based on the SSR restriction of the best-subset procedure which assured that none of them had over-fitting effects, plus a positive outcome in the hypothesis test of 1:1 correspondence. Table 2 shows the variables selected at each of them: the general model developed for the whole data without pre-stratification, and each FST-specific model developed for the even and uneven sized forest structures and oligophotic/closed canopy and euphotic/open canopy areas, obtained from the direct classification of airborne LiDAR data. While all the selected predictors were those typically included in LiDAR-AGB modelling – averages (e.g. quadratic or cubic means), dispersion statistics (e.g., variance), percentiles, and cover metrics (i.e. percentages above thresholds) of LiDAR return heights –, we identified critical differences in the metrics selected at each stratum, which is useful to understand what predictor variables are more important for estimating AGB at each area of a forest. We observed that higher LiDAR height percentiles were more relevant at open canopies and heterogeneous forests, whereas closed canopies in homogeneous forests obtained a best subset based on combinations of cover metrics and percentiles around the median. In the uneven-sized structures, higher percentiles, variance and absolute average deviation of

Table 3

Accuracy assessment of the observed and predicted aboveground biomass of the general model.

	Whole Data	$GC_H(L_{cv})$		L_{skew}	
		Even (<0.33)	Uneven (>0.33)	Oligophotic (<0)	Euphotic (>0)
Sample size	244	120	124	119	125
MD	-3.55	-2.09	-4.97	-4.56	-4.31
MD (%)	-3.95	-2.33	-5.54	-5.08	-4.81
RMSD	37.4	37.1	37.6	37.6	37.3
RMSD (%)	41.7	41.4	41.9	41.9	41.6
SSR	1.03	1.02	1.04	1.04	0.98

$GC_H(L_{cv})$: Gini coefficient/L-coefficient of variation of LiDAR heights; L_{skew} : L-skewness of LiDAR heights; MD: mean difference; RMSD: relative mean square difference;

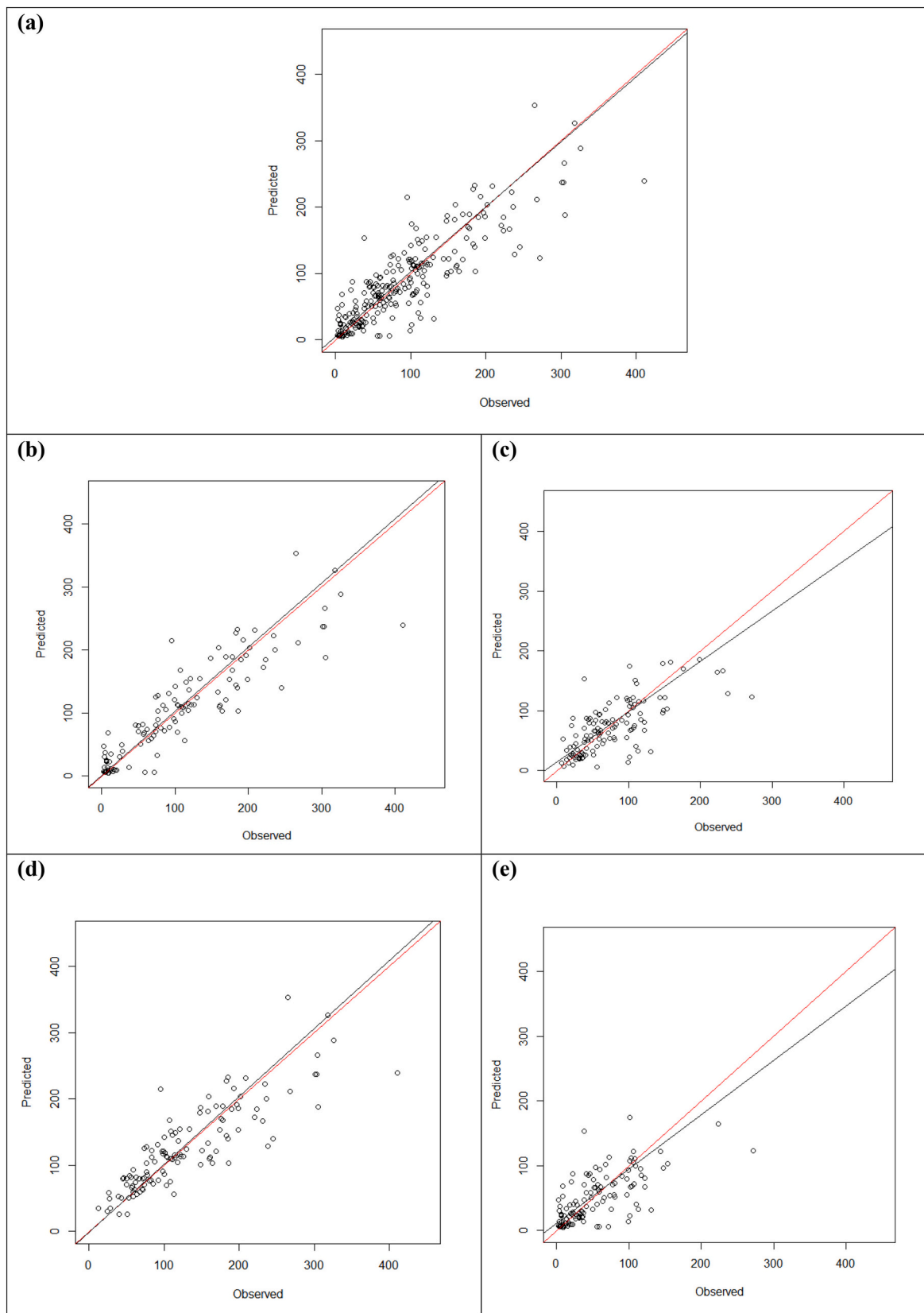


Fig. 6. Observed vs predicted aboveground biomass ($\text{Mg} \cdot \text{ha}^{-1}$) plots of the kNN imputation method using general model for (a) whole data without pre-stratification and each forest structural types obtained directly from airborne LiDAR classification such as (b) even sized, (c) uneven sized, (d) oligophotic/closed canopy and (e) euphotic/open canopy. The red line represents 1:1 correspondence and the black line shows linear regression fit between observed and predicted values. (For interpretation of the references to colour in this figure legend, the reader is referred to the web version of this article.)

Table 4

Accuracy assessment of the observed and predicted aboveground biomass of each forest structural type specific models.

(a) Even versus uneven-sized structure			
	Whole Data	$GC_H(L_{cv})$	
		Even (<0.33)	Uneven (>0.33)
Sample size	244	120	124
MD	-2.52	-2.30	-2.72
MD (%)	-2.81	-2.57	-3.03
RMSD	34.9	34.6	35.3
RMSD (%)	38.9	38.6	39.4
SSR	0.97	0.96	0.99

(b) Oligophotic/closed canopy versus euphotic/open canopy areas			
	Whole Data	L_{skew}	
		Oligophotic (<0)	Euphotic (>0)
Sample size	244	119	125
MD	-2.37	-2.22	-2.52
MD (%)	-2.64	-2.48	-2.81
RMSD	33.2	33.5	32.9
RMSD (%)	37.0	37.4	36.7
SSR	0.98	0.98	0.98

$GC_H(L_{cv})$: Gini coefficient/L-coefficient of variation of LiDAR heights; L_{skew} : L-skewness of LiDAR heights; MD: mean difference; RMSD: relative mean square difference; SSR: sum of square ratio.

LiDAR return heights were selected. On the other hand, in the even-sized stratum, the model included the mode, L_{skew} , the median and cover metrics (percentage of all returns above mode and total first returns). Similarly, in the oligophotic/closed canopy areas, the median and cover metrics were important, while in the euphotic areas/open canopy areas, higher percentiles and mean absolute deviation from median and variance were selected. Thus, the similarities of even-sized with oligophotic areas on one hand, and uneven with euphotic areas observed in Fig. 4, showed an influence in the modelling itself (Table 2), thus indicating convergence in the relationships between structure and modelling results.

3.3. Modelling aboveground biomass from airborne LiDAR based forest structural types

The AGB was predicted in each model using the associated best subset of LiDAR predictors, and their accuracies were assessed. In the general model (Table 3 and Fig. 6), i.e. a model fitted using the whole dataset, the RMSD between the observed and predicted AGB was $37.4 \text{ Mg} \cdot \text{ha}^{-1}$. We disaggregated these accuracy statistics by strata, to allow direct comparison with the FST-specific models, which resulted in 37.1 and $37.6 \text{ Mg} \cdot \text{ha}^{-1}$, in the even and uneven-sized forest areas and 37.6 and $37.3 \text{ Mg} \cdot \text{ha}^{-1}$ in oligophotic and euphotic areas, respectively. In relative terms, the general model RMSD 41.7%, which seems high because of the inclusions of seedling and sapling areas of very low AGB in the dataset. The general model showed some bias when applied to specific FSTs, as it can be appreciated by underpredictions of around 4.8–5.5% in terms of their MDs, with the even-sized forests being the only areas where not such strong bias effect was observed (-2.33% only).

The results for the FTS-specific models are summarized in Table 4a-b, and the scatterplots in Figs. 7-8. The RMSD improved both in the even sized ($34.6 \text{ Mg} \cdot \text{ha}^{-1}$) and uneven sized ($35.3 \text{ Mg} \cdot \text{ha}^{-1}$) forest structures (Table 4a) as compared to the general model (Table 3). The MD similarly improved in the uneven sized forest structure ($-2.72 \text{ Mg} \cdot \text{ha}^{-1}$) and only slightly decreased in the even sized areas ($-2.30 \text{ Mg} \cdot \text{ha}^{-1}$). These specific models developed for the even and uneven sized forest structures also showed an improvement in the MD and RMSD when aggregated for the whole area (-2.52 and $34.9 \text{ Mg} \cdot \text{ha}^{-1}$) (Table 4a),

compared to the general model (-3.55 and $37.4 \text{ Mg} \cdot \text{ha}^{-1}$) (Table 3). Similar improvements in the MD and RMSD were observed in the FST specific models developed for the oligophotic/closed canopy areas (-2.22 , $33.5 \text{ Mg} \cdot \text{ha}^{-1}$), euphotic areas/open canopies (-2.52 , $32.9 \text{ Mg} \cdot \text{ha}^{-1}$), and whole data (-2.37 , $33.2 \text{ Mg} \cdot \text{ha}^{-1}$) (Table 4b). All the FST-specific modelling approaches, thus, showed improvements compared to the general model both in terms of unbiasedness and improving the precision of predictions.

4. Discussion

4.1. Determining maximum entropy from a distribution of heights in 3D remote sensing

In previous contributions we have showed a threshold of interest which flags up maximum entropy at the Gini Coefficient value of $GC_{BA} = 0.50$ (Valbuena et al., 2012, 2017a). This threshold allows to compare the entropy of the ecosystem using a statistic of dispersion, arguing that is more correct for continuous variables because it avoids the factitious binning step required when computing foliage height diversity (McArthur and McArthur, 1961), based on Shannon's entropy index which was originally meant for discrete variables (Shannon, 1948). It is important to note that this threshold is applicable for a Gini coefficient of a Lorenz curve representing differences in basal area among trees growing within a given area (GC_{BA}) (Valbuena et al., 2012). On the other hand, in this contribution we further argue that for a Gini coefficient of a Lorenz curve representing differences in LiDAR heights within that same area (GC_H), the alternative value of $GC_H = 0.33$ should be the one used instead to identify maximum entropy. The reason is that height is a one-dimensional variable (X), whereas basal areas are two-dimensional (X^2). In order to achieve these generalized conclusions, we need to use theoretical distribution functions and show how their parameters propagate into Lorenz curves and values of the Gini Coefficient directly dependent on those parameters. In the Appendix A, we show formal proofs for these values obtained from theoretical distributions, to illustrate the reasoning employed in this contribution. We also show how these maxim entropy values of GC_X extend to higher dimensions (e.g. GC_{X^2}), thus developing a mathematical framework which provides unified means for determining maximum entropy in the 3D space of information provided by remote sensing tools such as LiDAR. Fig. 5 illustrates empirically the equivalence of the LiDAR and field approaches.

4.2. Rule-based pre-stratification into different forest structural types

Airborne LiDAR explains the key characteristics of forests related to the structural heterogeneity that can be relevant to describe tree size hierarchy (Valbuena et al., 2013), vegetation growth (Stark et al., 2012) and light availability (Lefsky et al., 2002a). Advancement in airborne LiDAR remote sensing promises reliable accuracies in the prediction of biophysical stand properties (Lefsky et al., 2002b; Valbuena et al., 2020) and various studies have evaluated and found that the pre-stratification of forests using airborne LiDAR can improve the attribute estimation (Nasset, 2002; Maltamo et al., 2015) and reduce the sampling efforts (Papa et al., 2020). Following the same concept but using solely the LiDAR data as opposed to using field information, in this study different FST were obtained from the direct classification of airborne LiDAR data. We applied rule-based pre-stratifications and used $L_{cv}(GC_H)$ and L_{skew} of the LiDAR echo heights which are the two prominent LiDAR metrics in separating the even from uneven sized structures and oligophotic/closed canopy from euphotic/open canopy forest areas, respectively (Valbuena et al., 2017a). In Fig. 4a, we found that the young, advanced and mature development classes which have similar diameters and basal areas distributions ($GC_{BA} < 0.5$) usually backscatter most of the LiDAR returns and hold smaller variance in their height values were mostly separated by the lower values of $L_{cv}(GC_H) < 0.33$. There is a consistency on results

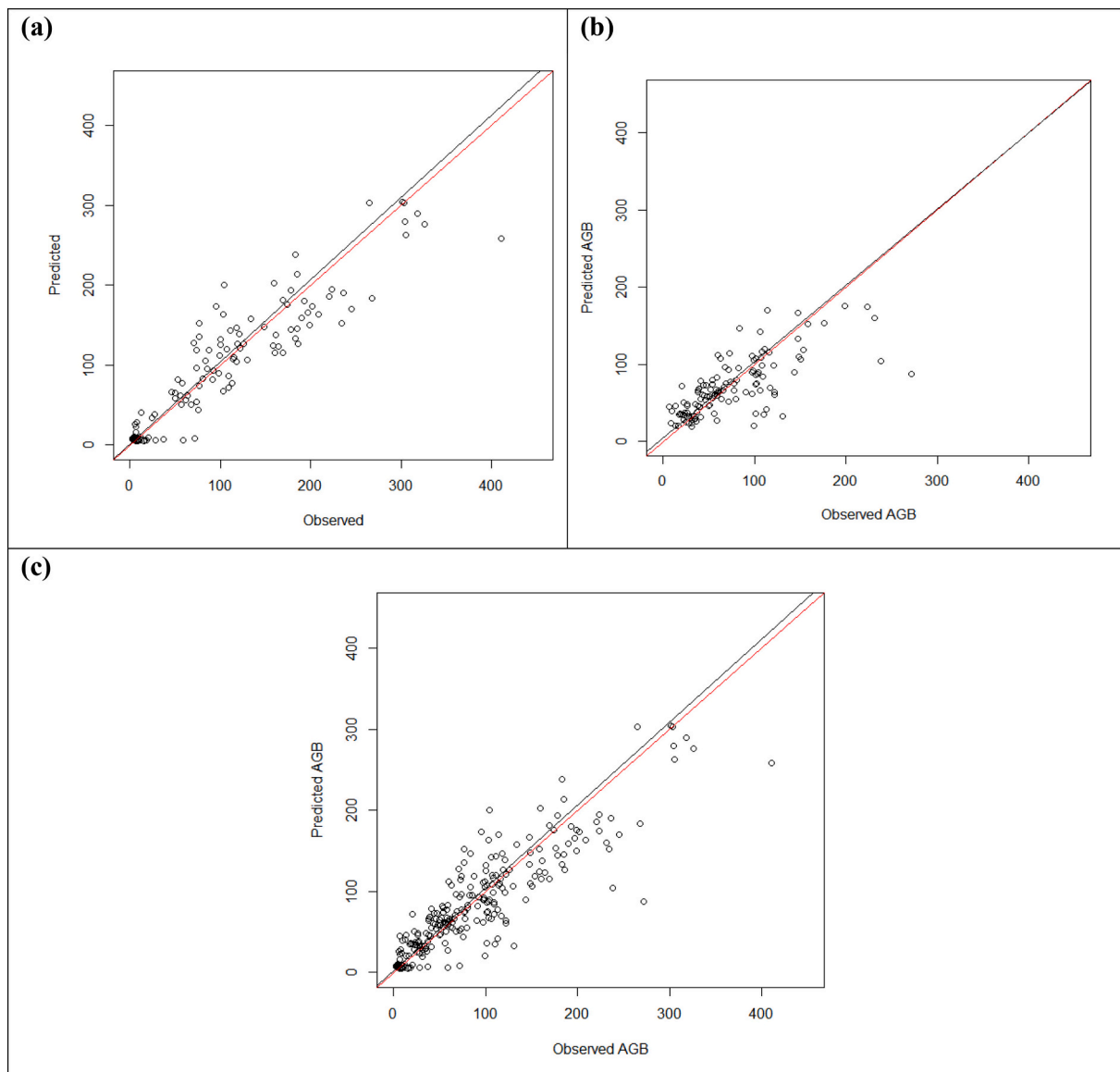


Fig. 7. Observed vs predicted aboveground biomass ($\text{Mg}\cdot\text{ha}^{-1}$) plots of the kNN imputation method using specific models developed for (a) even sized and (b) uneven sized forest structure and their combination for the (c) whole data. The red line represents 1:1 correspondence and the black line shows linear regression fit between observed and predicted values. (For interpretation of the references to colour in this figure legend, the reader is referred to the web version of this article.)

in Table 1 showing that LiDAR values of GC_H are reflected by higher values in GC_{BA} , with the proofs in Appendix A being the explanation for this effect. A notable exception is observed in the case of the sapling development, which showed a high uncertainty in terms of GC , with a wide range of values in both GC_{BA} and GC_H (Table 1). This is the reason that L_{skew} was important to add as an additional LiDAR metric because the similarity between GC_{BA} (Valbuena et al., 2013) and GC_H (L_{cv}) only occurs if the higher values of GC is due to the presence of canopy gaps which allow large a portion of laser pulses to pass and disperse in the canopy (Stark et al., 2012; Valbuena et al., 2017a). Thus, by looking at the L_{skew} values, the sapling was separated as euphotic/open canopy areas ($L_{skew} > 0$) which could be the reason of the higher L_{cv} values. Other development classes such as seed-tree and multi-storey areas were separated as uneven sized by both GC_{BA} (0.73 and 0.92) and GC_H ($L_{cv} = 0.58$ and 0.58), however, the shelterwood development class wherein the mean GC_{BA} was 0.95 was not properly separated and many plots were below $L_{cv}(GC_H) = 0.33$ (Fig. 4 and Table 1). This might be due to the omission of the understory vegetation by the lower point density of the ALS data in our study area ($0.91 \text{ points}\cdot\text{m}^{-2}$) and any pointy density

lower than at least $3 \text{ points}\cdot\text{m}^{-2}$ are unsuitable for the structural heterogeneity assessment, using the GC in particular (Adnan et al., 2017). Thus, the disintegration of such classes could further be improved by increasing the pulse density of the LiDAR data (Gobakken and Næsset, 2008; Ruiz et al., 2014).

When laser pulses hit a closed canopy vegetation, only a small portion of pulses penetrate the canopy, which is represented by LiDAR height distributions with negative asymmetry $L_{skew} < 0$. This also indicates the shady/oligophotic areas where only a smaller portion of light will reach the ground, for example, young, advance and mature development classes. Similarly, areas where smaller portion of LiDAR returns due to the presence of sparse vegetation denotes the open/euphotic areas which were detected by $L_{skew} > 0$, for example, seedlings, saplings, seed trees, shelterwood and multi-storey (Fig. 4b and Table 1). Fig. 5 further highlights the importance of this rule-based classification and presents an adequate comparison between the even and uneven sized forest structures separated by the $GC_H(L_{cv}) = 0.33$, or $GC_{BA} = 0.5$ (Appendix A). In this figure, it is clear that the diameter and basal area weighted distributions in both even sized and uneven sized structure

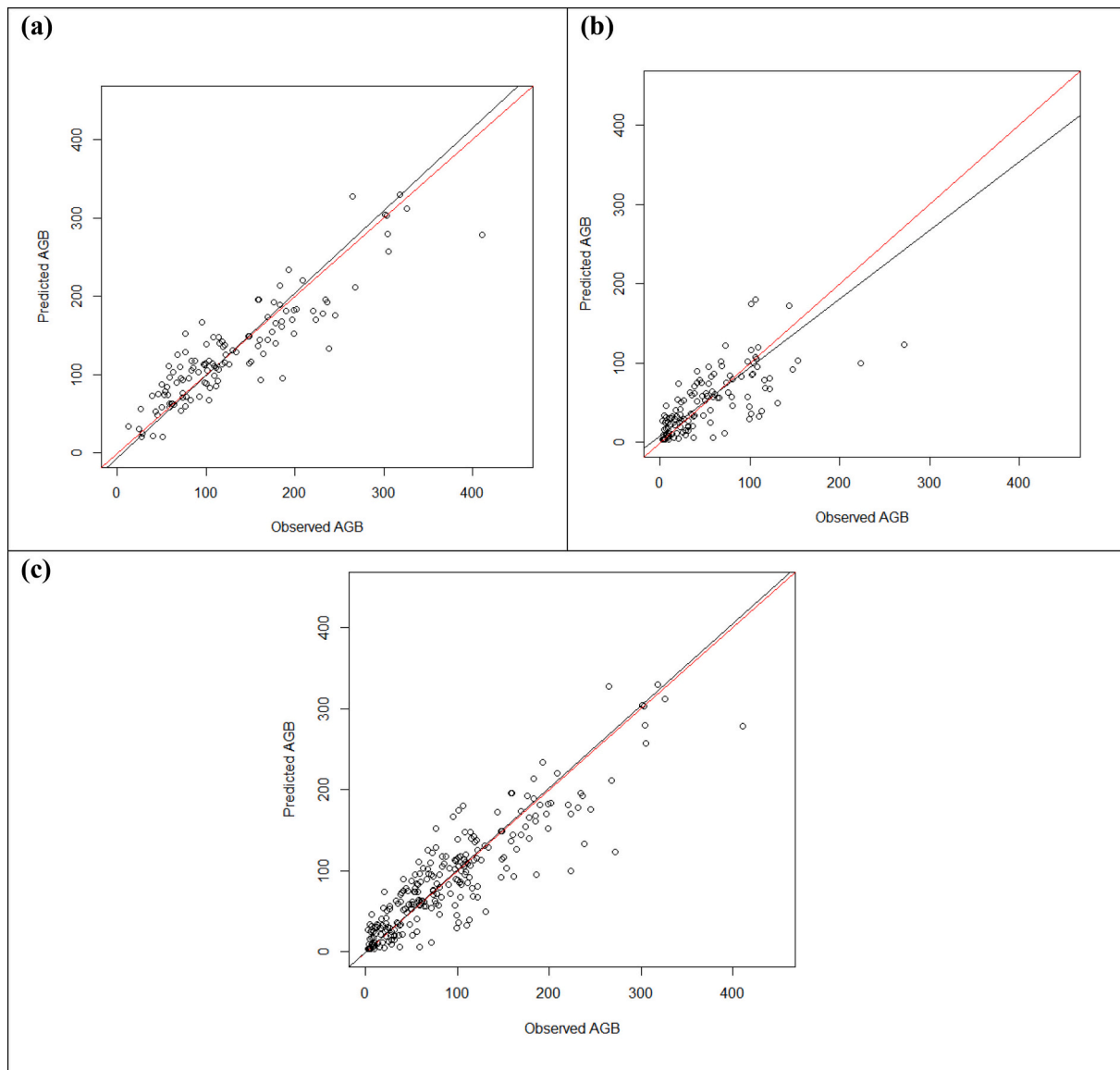


Fig. 8. Observed vs predicted aboveground biomass ($\text{Mg} \cdot \text{ha}^{-1}$) plots of the kNN imputation method using specific models for (a) oligophotic areas/closed canopies and (b) euphotic areas/open canopies and their combination for the (c) whole data. The red line represents 1:1 correspondence and the black line shows linear regression fit between observed and predicted values. (For interpretation of the references to colour in this figure legend, the reader is referred to the web version of this article.)

which are obtained from the GC_H (Fig. 5a and b) and GC_{BA} (Fig. 5c and d) are very similar and the small differences are due to missing detection of seedling in the smallest size class. This provides further insights that GC_H is an appropriate option to separate structural heterogeneity of forest.

4.3. Selection of best subsets of airborne LiDAR predictors in the AGB prediction models

Various alternatives are used to select the optimum number of parameters (predictors) to predict a response variable such as best subset, stepwise, and nearest neighbor (MSN) selection methods (Næsset, 2002; Van Aardt et al., 2008; Asner et al., 2010; Valbuena et al., 2017b; Almeida et al., 2019a). We used the best subset method in which the selection of a given variable is independent of interactions among variables as they are selected (Hudak et al., 2006). Thus, the selection of the six predictors was independent from the other LiDAR metrics and the different modelling options, yet reaching several convergences.

Minimizing the number of meaningful predictors that describe various aspects of the forest structures is an important consideration (Hudak et al., 2006; Asner and Mascaro, 2014; Vincent et al., 2014; Bouvier et al., 2015; Valbuena et al., 2017b), and our selection of six predictors to allow model comparison (Table 2) was a compromise balance between model error and overfitting that worked well for all the options. The results obtained in variable selection are as valuable as the accuracy assessment itself, since it shows convergences between some areas of the forest and discrepancies between opposing FSTs. They also show which FSTs influence more the general model, with effects both in the overall error but also bias effects in the areas of the forest that had a lower influence in the composition of the general model. Cover metrics were important in all models but more predominant in oligophotic areas. The variance of LiDAR return heights was only selected in the uneven sized structures and euphotic/open canopy areas. Different height percentiles were influential in different FST-specific models, with the median (50th height percentile) being important in the even sized and oligophotic structures, and higher percentiles (70th or 99th, representing dominant

trees) becoming selected in the uneven sized structure and euphotic areas (Adnan et al., 2017). Most importantly, the variables selected in the general model were highly influenced by the even-sized areas of the forest, with both models presenting large similarities (Table 2), which is a good explanation for the results observed in the accuracy assessment, since the general model showed lesser error in those areas and high levels of biasness in the remaining FSTs. All these demonstrate the superiority of obtaining FST-specific models to predict forest AGB from LiDAR, as opposed to approaches seeking a single model valid for all forest areas.

4.4. Comparison of the aboveground biomass predicted in the whole data without stratification and each pre-stratified FSTs

In addition to the typical statistics employed to evaluate the quality of AGB predictions, namely MD and RMSD (Van Aardt et al., 2008; Kankare et al., 2013; Straub et al., 2013; Rätty et al., 2018), we also employed an evaluation of the inflation of error in cross-validation (the SSR) and hypothesis test of 1:1 correspondence between observed and predicted AGB to enhance the reliability of our resulting models (Valbuena et al., 2017b). Considering the results obtained for whole dataset with either alternative, the $37.4 \text{ Mg}\cdot\text{ha}^{-1}$ RMSD of the general model (Table 3), was improved by the FST-specific model approaches, reaching $34.9 \text{ Mg}\cdot\text{ha}^{-1}$ (Table 4a), and $33.2 \text{ Mg}\cdot\text{ha}^{-1}$ (Table 4b). Considering results obtained by FST, all figures also show improvements, even and even-sized areas where RMSDs improved from the $37.1 \text{ Mg}\cdot\text{ha}^{-1}$ (Table 3) to $34.6 \text{ Mg}\cdot\text{ha}^{-1}$ (Table 4a), with only a slight increase in MD. This is very important, as otherwise result in FST-wise MDs for the general model showed bias effects in the highly structured forest areas. This is explained by the higher influence that even-sized areas had in the general model, possibly because LiDAR metrics have a larger explanatory capacity for AGB in these areas, thus showing potential harmful consequences in AGB modelling approaches neglecting the effects of forest structure. While the accuracies in AGB prediction improved only moderately in the FST-specific models as compared to the general model, the differences observed in the selection of airborne LiDAR predictors in each model can be critical, as they can produce biased results at specific areas of the forest. We thus encourage the prior classification into different FSTs for selecting the most relevant LiDAR predictors at each area of the forest, which besides of improving the estimation of AGB could provide important ecological insights on forest dynamics such as regeneration (Valbuena et al., 2013), self-thinning (Coomes and Allen, 2007) or productivity (Bourdier et al., 2016), and reduce the sampling efforts needed for a given level of accuracy (Papa et al., 2020), assisting in better forest inventory, management and planning (Næsset, 2002; Maltamo et al., 2015). Thus, the improved AGB

prediction approach is suitable for purposes such as quantification of carbon stock for REDD activities for a large forest area, but also for a better forest management, planning and understanding of the natural dynamics within a large forest area.

5. Conclusions

Our results demonstrate the superiority of obtaining FST-specific models to predict forest AGB from LiDAR, as opposed to approaches seeking a single model valid for all forest areas. We recommend the use of LiDAR information to pre-stratify the forest area prior to the field campaign, so that forest data acquisition can be tailored to the structural characteristics of the area. In order to determine these structural characteristics, we defended the use of GC above the use of FHD, being less computationally demanding but also conceptually better. Appendix A provides a mathematical framework for determining maximum entropy in 3D remote sensing datasets based on the GC of theoretical continuous distributions, intended to replace FHD as entropy measure in one-dimensional LiDAR vertical profiles (1D), with extensions to higher order dimensions bi- or three-dimensional (2D or 3D).

CRedit authorship contribution statement

Syed Adnan: Conceptualization; Data curation; Methodology; Formal analysis; Writing - original draft. **Matti Maltamo:** Supervision; Writing - review & editing. **Lauri Mehtätalo:** Methodology. **Rhei N. L. Ammatturo:** Methodology. **Petteri Packalen:** Writing - review & editing. **Rubén Valbuena:** Conceptualization; Methodology; Writing - review & editing; Supervision.

Declaration of Competing Interest

The authors declare that they have no known competing financial interests or personal relationships that could have appeared to influence the work reported in this paper.

Acknowledgements

Rhei N. L. Ammatturo worked at the Department of Plant Sciences supervised by Rubén Valbuena, under The Cambridge Earth System Sciences Doctoral Training Partnerships (Cambridge ESS DTP, reference NE/L002507/1), which is a scheme funded by the UK Natural Environment Research Council (NERC). We would like to thank the Editor-in-Chief, Associate Editor and three reviewers for their comments and suggestions for the manuscript.

Appendix A. Proofs for maximum entropy thresholds corresponding to $GC_X = 0.33$ and $GC_{X^2} = 0.50$

Let X be a random variable taking values in the set of positive numbers, and $E[X]$ its expectation. Let $f_X(x)$ and $F_X(x)$ be their probability density function (p.d.f.) and cumulative distribution function (c.d.f.), respectively, and further let $F_X^{-1}(p)$ be the quantile function (inverse of the c.d.f.; its generalized definition is $F_X^{-1}(p) = \inf \{x : p \leq F(x)\}$). The Lorenz curve $L_X(p)$ specifies the accumulated proportion of the total of X that is attributed to a given accumulated share of the population ordered by increasing X . Thus, the Lorenz curve provides a mapping from interval $[0,1]$ to interval $[0,1]$, where the domain includes the proportion from the ordered population and the codomain the share of X . The Lorenz curve can be written as

$$L_X(p) = \frac{\int_0^p F^{-1}(t)dt}{E[X]}, \text{ for } 0 \leq p \leq 1 \quad (\text{A.1})$$

The Gini coefficient is the twice area between the Lorenz curve and the diagonal line $L_X(p) = p$, which is thus assessed with the integral:

$$GC_X = 1 - 2 \int_0^1 L_X(p)dp \quad (\text{A.2})$$

The Lorenz curve for aX for a positive constant a is the same as that of X . Therefore the Lorenz curve and Gini coefficient have the property of being invariant under linear scaling of X by a positive constant.

In applications using the distribution LiDAR heights $X = H$, the Lorenz curve $L_H(p)$ specifies the proportion of total accumulated heights at the 100p

% of lower (or higher) vertical strata. In forest science, from the distribution of tree diameters $X = D$, the Lorenz curve $L_D(p)$ gives the proportion of total accumulated diameters for the 100p % smallest (or largest) trees. It is however more common to use variables which are logical to accumulate, such as basal area $X = BA$ or above-ground biomass $X = AGB$, as it is more useful to know the proportion of basal area or biomass accumulated from for the 100p % smallest (or largest) trees. These variables are however never measured directly, and instead derived from a transformation of D or H , or both (Mehrtälö and Lappi, 2020). The following proofs demonstrate: (1) the threshold $GC_X = 0.33$ denotes maximum entropy for unidimensional measures, i.e. D or H ; and (2) that this value of maximum entropy for D derives into $GC_{X^2} = 0.50$ for the transformed variable $Z = X^2$, namely the bi-dimensional measure BA , as it was empirically devised in Valbuena et al. (2012).

Proofs for the Lorenz curve and Gini Coefficient of a uniformly distributed variable (maximum entropy).

The continuous uniform distribution $U(x_{\max}, x_{\min})$ has equal probability density for any u -length interval $[x, x + u]$ within the range $X \in [x_{\min}, x_{\max}]$. It has the maximum entropy among all continuous distributions which have the same range (Sung and Bera, 2009). Thus, for a given range $\theta = x_{\max} - x_{\min}$ and a given number of strata θ/u considered, the uniform distribution yields the maximum value of Shannon’s (1848) entropy index (Valbuena et al., 2012). In applications using LIDAR heights, this is a vertical profile showing even proportions for all strata, yielding a maximum value for McArthur and McArthur’s (1961) foliage height diversity, with $x_{\min} = 0$ being the ground level and $x_{\max} = \theta$ being the maximum height of vegetation.

The continuous uniform distribution $X \sim U(0, \theta)$ has the p.d.f.:

$$f_X(x; \theta) = \begin{cases} 1/\theta, & \text{for } 0 \leq x \leq \theta \\ 0, & \text{otherwise} \end{cases} \tag{A.3}$$

The c.d.f. is:

$$F_X(x; \theta) = \begin{cases} 0, & \text{for } x < 0 \\ x/\theta, & \text{for } 0 \leq x \leq \theta \\ 1, & \text{for } \theta \leq x \end{cases} \tag{A.4}$$

The quantile function and expected value are:

$$F_X^{-1}(p) = \theta p \tag{A.5}$$

$$E[X](= \mu) = \frac{\theta}{2} \tag{A.6}$$

Substituting these in Eq. (A.1), the Lorenz curve becomes (Fig. A1):

$$L_X(p) = \frac{\int_0^p \theta t dt}{\theta/2} = \frac{\theta p^2/2}{\theta/2} = p^2 \tag{A.7}$$

And thus, substituting in Eq. (A.2), the Gini coefficient of a uniform distribution becomes:

$$GC_X = 1 - 2 \int_0^1 p^2 dp = 1 - \frac{2}{3} = \frac{1}{3} \tag{A.8}$$

Hence, any variable X that has the minimum of zero and is distributed evenly along all its values, such as D or H , would have $GC_X = 0.33$, which thus is the value of Gini Coefficient which corresponds to maximum entropy.

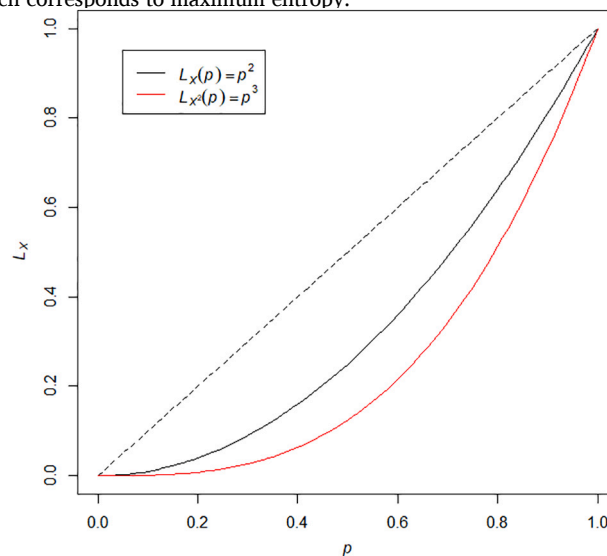


Fig. A1. Lorenz curves of maximum entropy for X , and its transformed variable $Z \propto X^2$.

Proofs for the Lorenz curve and Gini Coefficient of the second power of uniformly distributed variable.

Next, we will proceed to deduce the Lorenz curves $L_{BA}(p)$ and Gini coefficient GC_{BA} values for basal areas that derive from this situation of maximum entropy in the distribution of tree diameters. The basal area is directly calculated from a transformation of the diameters $BA = aD^2$. As per

the scale-invariability property of Lorenz curves the scalar a can be further disregarded, and thus we now consider the Lorenz curve and Gini coefficient of transformation $Z = X^2$ when $X \sim U(0, \theta)$.

The c.d.f. and p.d.f of the transformed variable are:

$$F_{X^2}(z; \theta) = \begin{cases} 0, & \text{for } z \leq 0 \\ \sqrt{z}/\theta, & \text{for } 0 \leq z \leq \theta^2 \\ 1, & \text{for } z \geq \theta^2 \end{cases} \quad (\text{A.9})$$

$$f_{X^2}(z; \theta) = \begin{cases} \frac{1}{2\theta\sqrt{z}}, & \text{for } 0 \leq z \leq \theta^2 \\ 0, & \text{otherwise} \end{cases} \quad (\text{A.10})$$

Thus, the quantile function and expected value of Z are:

$$F_{X^2}^{-1}(p) = \theta^2 p^2 \quad (\text{A.11})$$

$$E[X^2] = \frac{\theta^2}{3} \quad (\text{A.12})$$

Substituting these in Eq. (A.1), the Lorenz curve becomes (Fig. A1):

$$L_{X^2}(p) = \frac{\int_0^p \theta^2 t^2 dt}{\theta^2/3} = \frac{\theta^2 p^3/3}{\theta^2/3} = p^3 \quad (\text{A.13})$$

And thus, substituting in Eq. (A.2), the Gini coefficient of a uniform distribution becomes:

$$GC = 1 - 2 \int_0^1 p^3 dp = 1 - \frac{2}{4} = \frac{1}{2} \quad (\text{A.14})$$

Hence, for any variable $Z \propto X^2$ that is proportional to the second power of X , such as of BA is to D , the $GC_{X^2} = 0.50$ corresponds to the maximum entropy of X .

References

- Adnan, S., Maltamo, M., Coomes, D.A., Valbuena, R., 2017. Effects of plot size, stand density, and scan density on the relationship between airborne laser scanning metrics and the Gini coefficient of tree size inequality. *Can. J. For. Res.* 47 (12), 1590–1602.
- Adnan, S., Maltamo, M., Coomes, D.A., García-Abril, A., Malhi, Y., Manzanera, J.A., Butt, N., Morecroft, M., Valbuena, R., 2019. A simple approach to forest structure classification using airborne laser scanning that can be adopted across bioregions. *For. Ecol. Manag.* 433, 111–121.
- Almeida, D.R.A., Stark, S.C., Chazdon, R., Nelson, B.W., César, R.G., Meli, P., Gorgens, E. B., Duarte, M.M., Valbuena, R., Moreno, V.S., Mendes, A.F., 2019a. The effectiveness of lidar remote sensing for monitoring forest cover attributes and landscape restoration. *For. Ecol. Manag.* 438, 34–43.
- Almeida, D.R.A., Stark, S.C., Silva, C.A., Hammamura, C., Valbuena, R., 2019b. leafR: a set of functions for analyzing the structure of forests based on the leaf area density (LAD) and leaf area index (LAI) measures calculated from Airborne Laser Scanning (ALS). In: R Package. Version 0.3. CRAN - The Comprehensive R Archive Network.
- Asner, G.P., Mascaro, J., 2014. Mapping tropical forest carbon: calibrating plot estimates to a simple LiDAR metric. *Remote Sens. Environ.* 140, 614–624.
- Asner, G.P., Powell, G.V., Mascaro, J., Knapp, D.E., Clark, J.K., Jacobson, J., Kennedy-Bowdoin, T., Balaji, A., Paez-Acosta, G., Victoria, E., Secada, L., 2010. High-resolution forest carbon stocks and emissions in the Amazon. *Proc. Natl. Acad. Sci.* 107 (38), 16738–16742.
- Bakx, T.R., Koma, Z., Seijmonsbergen, A.C., Kissling, W.D., 2019. Use and categorization of light detection and ranging vegetation metrics in avian diversity and species distribution research. *Divers. Distrib.* 25 (7), 1045–1059.
- Bollandsås, O.M., Næsset, E., 2007. Estimating percentile-based diameter distributions in uneven-sized Norway spruce stands using airborne laser scanner data. *Scand. J. For. Res.* 22 (1), 33–47.
- Boudreau, J., Nelson, R.F., Margolis, H.A., Beaudoin, A., Guindon, L., Kimes, D.S., 2008. Regional aboveground forest biomass using airborne and spaceborne LiDAR in Québec. *Remote Sens. Environ.* 112 (10), 3876–3890.
- Bourdiar, T., Cordonnier, T., Kunstler, G., Piedallu, C., Lagarrigues, G., Courbaud, B., 2016. Tree size inequality reduces forest productivity: an analysis combining inventory data for ten European species and a light competition model. *PLoS One* 11 (3) e0151852.
- Bouvier, M., Durrieu, S., Fournier, R.A., Renaud, J.P., 2015. Generalizing predictive models of forest inventory attributes using an area-based approach with airborne LiDAR data. *Remote Sens. Environ.* 156, 322–334.
- Brokaw, N.V.L., Lent, R.A., 1999. Vertical structure. In: 'Maintaining Biodiversity in Forest Ecosystems' (Eds I. Hunter and L. Malcom.). Cambridge University Press, Cambridge, UK, pp. 373–399.
- Coomes, D.A., Allen, R.B., 2007. Effects of size, competition and altitude on tree growth. *J. Ecol.* 95 (5), 1084–1097.
- Crespo-Peremarch, P., Fournier, R.A., Nguyen, V.T., van Lier, O.R., Ruiz, L.Á., 2020. A comparative assessment of the vertical distribution of forest components using full-waveform airborne, discrete airborne and discrete terrestrial laser scanning data. *For. Ecol. Manag.* 473, 118268.
- Crookston, N.L., Finley, A.O., 2008. yalmpute: an R package for kNN imputation. *J. Stat. Softw.* 23 (10), 1–16.
- Drake, J.B., Knox, R.G., Dubayah, R.O., Clark, D.B., Condit, R., Blair, J.B., Hofton, M., 2003. Above-ground biomass estimation in closed canopy neotropical forests using lidar remote sensing: factors affecting the generality of relationships. *Glob. Ecol. Biogeogr.* 12 (2), 147–159.
- Erdelen, M., 1984. Bird communities and vegetation structure: I. correlations and comparisons of simple and diversity indices. *Oecologia* 61 (2), 277–284.
- Fahey, R.T., Atkins, J.W., Gough, C.M., Hardiman, B.S., Nave, L.E., Tallant, J.M., Nadehoffer, K.J., Vogel, C., Scheuermann, C.M., Stuart-Haëntjens, E., Haber, L.T., 2019. Defining a spectrum of integrative trait-based vegetation canopy structural types. *Ecol. Lett.* 22 (12), 2049–2059.
- Gibbs, H.K., Brown, S., Niles, J.O., Foley, J.A., 2007. Monitoring and estimating tropical forest carbon stocks: making REDD a reality. *Environ. Res. Lett.* 2 (4), 045023.
- Gini, C., 1921. Measurement of inequality of incomes. *Econ. J.* 31 (121), 124–126.
- Gobakken, T., Næsset, E., 2008. Assessing effects of laser point density, ground sampling intensity, and field sample plot size on biophysical stand properties derived from airborne laser scanner data. *Can. J. For. Res.* 38 (5), 1095–1109.
- Görgens, E.B., Valbuena, R., Rodríguez, L.C., 2017. A method for optimizing height threshold when computing airborne laser scanning metrics. *Photogramm. Eng. Remote. Sens.* 83 (5), 343–350.
- Häbel, H., Kuronen, M., Henttonen, H.M., Kangas, A., Myllymäki, M., 2019. The effect of spatial structure of forests on the precision and costs of plot-level forest resource estimation. *Forest Ecosyst.* 6 (1), 8.
- Hagar, J.C., Yost, A., Haggerty, P.K., 2020. Incorporating LiDAR metrics into a structure-based habitat model for a canopy-dwelling species. *Remote Sens. Environ.* 236, 111499.
- Hall, S.A., Burke, I.C., Box, D.O., Kaufmann, M.R., Stoker, J.M., 2005. Estimating stand structure using discrete-return lidar: an example from low density, fire prone ponderosa pine forests. *For. Ecol. Manag.* 208 (1–3), 189–209.
- Hernando, A., Puerto, L., Mola-Yudego, B., Manzanera, J.A., García-Abril, A., Maltamo, M., Valbuena, R., 2019. Estimation of forest biomass components using airborne LiDAR and multispectral sensors. *iForest-Biogeosci. Forestry* 12 (2), 207.
- Hudak, A.T., Crookston, N.L., Evans, J.S., Falkowski, M.J., Smith, A.M., Gessler, P.E., Morgan, P., 2006. Regression modeling and mapping of coniferous forest basal area and tree density from discrete-return lidar and multispectral satellite data. *Can. J. Remote. Sens.* 32 (2), 126–138.
- Jaskierniak, D., Lane, P.N., Robinson, A., Lucieer, A., 2011. Extracting LiDAR indices to characterise multilayered forest structure using mixture distribution functions. *Remote Sens. Environ.* 115 (2), 573–585.

- Kankare, V., Vastaranta, M., Holopainen, M., Rätty, M., Yu, X., Hyyppä, J., Hyyppä, H., Alho, P., Viitala, R., 2013. Retrieval of forest aboveground biomass and stem volume with airborne scanning LiDAR. *Remote Sens.* 5 (5), 2257–2274.
- Knapp, N., Fischer, R., Cazcarra-Bes, V., Huth, A., 2020. Structure metrics to generalize biomass estimation from lidar across forest types from different continents. *Remote Sens. Environ.* 237, 111597.
- Koukoulas, S., Blackburn, G.A., 2005. Mapping individual tree location, height and species in broadleaved deciduous forest using airborne LIDAR and multi-spectral remotely sensed data. *Int. J. Remote Sens.* 26 (3), 431–455.
- Kronseider, K., Ballhorn, U., Böhm, V., Siegert, F., 2012. Above ground biomass estimation across forest types at different degradation levels in Central Kalimantan using LiDAR data. *Int. J. Appl. Earth Obs. Geoinf.* 18, 37–48.
- Lefsky, M.A., Cohen, W.B., Parker, G.G., Harding, D.J., 2002a. Lidar remote sensing for ecosystem studies: Lidar, an emerging remote sensing technology that directly measures the three-dimensional distribution of plant canopies, can accurately estimate vegetation structural attributes and should be of particular interest to forest, landscape, and global ecologists. *BioScience* 52 (1), 19–30.
- Lefsky, M.A., Cohen, W.B., Harding, D.J., Parker, G.G., Acker, S.A., Gower, S.T., 2002b. Lidar remote sensing of above-ground biomass in three biomes. *Glob. Ecol. Biogeogr.* 11 (5), 393–399.
- Leite, H.G., Tavares de Oliveira, F.H., 2002. Statistical procedure to test identity between analytical methods. *Commun. Soil Sci. Plant Anal.* 33 (7–8), 1105–1118.
- Lexerod, N.L., Eid, T., 2006. An evaluation of different diameter diversity indices based on criteria related to forest management planning. *For. Ecol. Manag.* 222, 17–28. <https://doi.org/10.1016/j.foreco.2005.10.046>.
- Lindenmayer, D.B., Cunningham, R.B., Donnelly, C.F., Franklin, J.F., 2000. Structural features of old-growth Australian montane ash forests. *For. Ecol. Manag.* 134 (1–3), 189–204.
- Listopad, C.M.C.S., Masters, R.E., Drake, J., Weishampel, J., Branquinho, C., 2015. Structural diversity indices based on airborne LiDAR as ecological indicators for managing highly dynamic landscapes. *Ecol. Indic.* 57, 268–279.
- Longo, M., Keller, M., dos Santos, M.N., Leitold, V., Pinagé, E.R., Baccini, A., Saatchi, S., Nogueira, L.M., Batistella, M., Morton, D.C., 2017. Aboveground biomass variability across intact and degraded forests in the Brazilian Amazon. *Glob. Biogeochem. Cycles* 33, 1639.
- Lovejoy, T.E., 1972. Bird species diversity and composition in Amazonian rain forests. *Am. Zool.* 12, 711–712.
- Lumley, T., Miller, A., 2017. Leaps: Regression Subset Selection. R Package Version, 3.0.
- Magnussen, S., Eggermont, P., LaRicca, V.N., 1999. Recovering tree heights from airborne laser scanner data. *For. Sci.* 45 (3), 407–422.
- Maltamo, M., Mustonen, K., Hyyppä, J., Pitkänen, J., Yu, X., 2004. The accuracy of estimating individual tree variables with airborne laser scanning in a boreal nature reserve. *Can. J. For. Res.* 34 (9), 1791–1801.
- Maltamo, M., Packalén, P., Yu, X., Erikäinen, K., Hyyppä, J., Pitkänen, J., 2005. Identifying and quantifying structural characteristics of heterogeneous boreal forests using laser scanner data. *For. Ecol. Manag.* 216 (1–3), 41–50.
- Maltamo, M., Ørka, H.O., Bollandsås, O.M., Gobakken, T., Næsset, E., 2015. Using pre-classification to improve the accuracy of species-specific forest attribute estimates from airborne laser scanner data and aerial images. *Scand. J. For. Res.* 30, 336–345.
- Mascaro, J., Litton, C.M., Hughes, R.F., Uowolo, A., Schnitzer, S.A., 2011. Minimizing bias in biomass allometry: model selection and log-transformation of data. *Biotropica* 43 (6), 649–653.
- McArthur, R.H., McArthur, J.W., 1961. On bird species diversity. *Ecology* 42, 594–598.
- McElhinny, C., Gibbons, P., Brack, C., Bauhus, J., 2005. Forest and woodland stand structural complexity: its definition and measurement. *For. Ecol. Manag.* 218 (1–3), 1–24.
- McGaughey, R., 2019. FUSION/LDV: Software for LIDAR Data Analysis and Visualization. Version 3.70. USDA Forest Service, Pacific Northwest Research Station (accessed December 2018).
- McInerney, D.O., Suarez-Minguez, J., Valbuena, R., Nieuwenhuis, M., 2010. Forest canopy height retrieval using LIDAR data, medium-resolution satellite imagery and k NN estimation in Aberfoyle, Scotland. *Forestry* 83 (2), 195–206.
- Mehtätalo, L., Lappi, J., 2020. Biometry for Forestry and Environmental Data: With Examples in R. Chapman and Hall/CRC, New York.
- Mehtätalo, L., Nyblom, J., 2009. Estimating forest attributes using observations of canopy height: a model-based approach. *For. Sci.* 55 (5), 411–422.
- Mehtätalo, L., Nyblom, J., 2012. A model-based approach for airborne laser scanning inventory: application for square grid spatial pattern. *For. Sci.* 58 (2), 106–118.
- Mononen, L., Auvinen, A.P., Packalén, P., Virkkala, R., Valbuena, R., Bohlin, I., Valkama, J., Vihervaara, P., 2018. Usability of citizen science observations together with airborne laser scanning data in determining the habitat preferences of forest birds. *For. Ecol. Manag.* 430, 498–508.
- Moran, C.J., Rowell, E.M., Seielstad, C.A., 2018. A data-driven framework to identify and compare forest structure classes using LiDAR. *Remote Sens. Environ.* 211, 154–166.
- Næsset, E., 2002. Predicting forest stand characteristics with airborne scanning laser using a practical two-stage procedure and field data. *Remote Sens. Environ.* 80 (1), 88–99.
- Næsset, E., Gobakken, T., 2008. Estimation of above- and below-ground biomass across regions of the boreal forest zone using airborne laser. *Remote Sens. Environ.* 112 (6), 3079–3090.
- Näslund, M., 1936. Skogsförsöksanstaltens gallringsförsök i tallskog. *Meddelanden från Statens Skogsförsöksanstalt* 29, 169.
- Neumann, M., Starlinger, F., 2001. The significance of different indices for stand structure and diversity in forests. *For. Ecol. Manag.* 145 (1–2), 91–106.
- Papa, D.A., de Almeida, D.R.A., Silva, C.A., Figueiredo, E.O., Stark, S.C., Valbuena, R., Rodriguez, L.C.E., d'Oliveira, M.V.N., 2020. Evaluating tropical forest classification and field sampling stratification from lidar to reduce effort and enable landscape monitoring. *For. Ecol. Manag.* 457, 117634.
- Pearson, D.L., 1975. The relation of foliage complexity to ecological diversity of three Amazonian bird communities. *Condor* 77 (4), 453–466.
- Piñeiro, G., Perelman, S., Guerschman, J.P., Paruelo, J.M., 2008. How to evaluate models: observed vs. predicted or predicted vs. observed? *Ecol. Model.* 216 (3–4), 316–322.
- R Core Team, 2019. R: A Language and Environment for Statistical Computing [Online]. R Foundation for Statistical Computing, Vienna, Austria. Available from: <http://www.R-project.org>.
- Rätty, J., Packalén, P., Maltamo, M., 2018. Comparing nearest neighbor configurations in the prediction of species-specific diameter distributions. *Ann. For. Sci.* 75 (1), 26.
- Repola, J., 2008. Biomass equations for birch in Finland. *Silva Fennica* 42 (1), 605–624.
- Repola, J., 2009. Biomass equations for scots pine and Norway spruce in Finland. *Silva Fennica* 43 (4), 625–647.
- Ruiz, L.A., Hermsilla, T., Mauro, F., Godino, M., 2014. Analysis of the influence of plot size and LiDAR density on forest structure attribute estimates. *Forests* 5 (5), 936–951. <https://doi.org/10.3390/f5050936>.
- Schneider, F.D., Morsdorf, F., Schmid, B., Petchey, O.L., Hueni, A., Schimel, D.S., Schaeppman, M.E., 2017. Mapping functional diversity from remotely sensed morphological and physiological forest traits. *Nat. Commun.* 8 (1), 1–12.
- Shannon, C.E., 1948. A mathematical theory of communication. *Bell Syst. Tech. J.* 27, 379–423 (and 623–656).
- Siipilehto, J., 1999. Improving the accuracy of predicted basal-area diameter distribution in advanced stands by determining stem number. *Silva Fenn* 33.
- Simonson, W.D., Allen, H.D., Coomes, D.A., 2014. Applications of airborne lidar for the assessment of animal species diversity. *Methods Ecol. Evol.* 5 (8), 719–729.
- Stark, S.C., Leitold, V., Wu, J.L., Hunter, M.O., de Castilho, C.V., Costa, F.R., McMahon, S.M., Parker, G.G., Shimabukuro, M.T., Lefsky, M.A., Keller, M., 2012. Amazon forest carbon dynamics predicted by profiles of canopy leaf area and light environment. *Ecol. Lett.* 15 (12), 1406–1414.
- Straub, C., Tian, J., Seitz, R., Reinartz, P., 2013. Assessment of Cartosat-1 and WorldView-2 stereo imagery in combination with a LiDAR-DTM for timber volume estimation in a highly structured forest in Germany. *Forestry* 86 (4), 463–473.
- Sung, P.Y., Bera, A.K., 2009. Maximum entropy autoregressive conditional heteroskedasticity model. *J. Econ.* 150 (2), 219–230. [CiteSeerX 10.1.1.511.9750](https://doi.org/10.1016/j.jeconom.2008.12.014).
- Valbuena, R., Packalén, P., Martín, S., Maltamo, M., 2012. Diversity and equitability ordering profiles applied to study forest structure. *For. Ecol. Manag.* 276, 185–195.
- Valbuena, R., Packalén, P., Mehtätalo, L., García-Abril, A., Maltamo, M., 2013. Characterizing forest structural types and shelterwood dynamics from Lorenz-based indicators predicted by airborne laser scanning. *Can. J. For. Res.* 43 (11), 1063–1074.
- Valbuena, R., Maltamo, M., Packalén, P., 2016. Classification of multilayered forest development classes from low-density national airborne lidar datasets. *Forestry* 89 (4), 392–401.
- Valbuena, R., Maltamo, M., Mehtätalo, L., Packalén, P., 2017a. Key structural features of boreal forests may be detected directly using L-moments from airborne lidar data. *Remote Sens. Environ.* 194, 437–446.
- Valbuena, R., Hernandez, A., Manzanera, J.A., Görgens, E.B., Almeida, D.R.A., Mauro, F., García-Abril, A., Coomes, D.A., 2017b. Enhancing of accuracy assessment for forest above-ground biomass estimates obtained from remote sensing via hypothesis testing and overfitting evaluation. *Ecol. Model.* 366, 15–26.
- Valbuena, R., O'Connor, B., Zellweger, F., Simonson, W., Vihervaara, P., Maltamo, M., Silva, C.A., Almeida, D.R.A., Danks, F., Morsdorf, F., Chirici, G., 2020. Standardizing ecosystem morphological traits from 3D information sources. *Trends Ecol. Evol.* <https://doi.org/10.1016/j.tree.2020.03.006>.
- Van Aardt, J.A., Wynne, R.H., Scriveri, J.A., 2008. Lidar-based mapping of forest volume and biomass by taxonomic group using structurally homogenous segments. *Photogramm. Eng. Remote Sens.* 74 (8), 1033–1044.
- Vierling, K.T., Vierling, L.A., Gould, W.A., Martinuzzi, S., Clawges, R.M., 2008. Lidar: shedding new light on habitat characterization and modeling. *Front. Ecol. Environ.* 6 (2), 90–98.
- Vincent, G., Sabatier, D., Rutishauser, E., 2014. Revisiting a universal airborne light detection and ranging approach for tropical forest carbon mapping: scaling-up from tree to stand to landscape. *Oecologia* 175 (2), 439–443.
- Weiner, J., Thomas, S.C., 1986. Size variability and competition in plant monocultures. *Oikos* 211–222.
- Weiner, J., 1990. Asymmetric competition in plant populations. *Trends Ecol. Evol.* 5 (11), 360–364. [https://doi.org/10.1016/0169-5347\(90\)90095-U](https://doi.org/10.1016/0169-5347(90)90095-U). PMID:21232393.
- Weisberg, P.J., Dilts, T.E., Becker, M.E., Young, J.S., Wong-Kone, D.C., Newton, W.E., Ammon, E.M., 2014. Guild-specific responses of avian species richness to lidar-derived habitat heterogeneity. *Acta Oecol.* 59, 72–83.
- Wilkes, P., Jones, S.D., Suarez, L., Haywood, A., Mellor, A., Woodgate, W., Soto-Berelov, M., Skidmore, A.K., 2016. Using discrete-return airborne laser scanning to quantify number of canopy strata across diverse forest types. *Methods Ecol. Evol.* 7 (6), 700–712.
- Zolkos, S.G., Goetz, S.J., Dubayah, R., 2013. A meta-analysis of terrestrial aboveground biomass estimation using lidar remote sensing. *Remote Sens. Environ.* 128, 289–298.